ELSEVIER

Nuclear Instruments and Methods in Physics Research A 489 (2002) 85–98

NUCLEAR INSTRUMENTS & METHODS IN PHYSICS RESEARCH Section A

www.elsevier.com/locate/nima

The effect of incremental gamma-ray doses and incremental neutron fluences upon the performance of self-biased ^{10}B-coated high-purity epitaxial GaAs thermal neutron detectors

H.K. Gersch[a], D.S. McGregor[a,*], P.A. Simpson[b]

[a] *Semiconductor Materials and Radiological Technologies Laboratory, Department of Nuclear Engineering and Radiological Sciences, University of Michigan, 2355 Bonisteel Boulevard, Ann Arbor, MI 48109-2104, USA*

[b] *Phoenix Memorial Laboratory, University of Michigan, Ann Arbor, MI 48109-2100, USA*

Received 11 July 2001; received in revised form 28 January 2002; accepted 12 February 2002

Abstract

High-purity epitaxial GaAs ^{10}B-coated thermal neutron detectors advantageously operate at room temperature without externally applied voltage. Sample detectors were systematically irradiated at fixed grid locations near the core of a 2 MW research reactor to determine their operational neutron dose threshold. Reactor pool locations were assigned so that fast and thermal neutron fluxes to the devices were similar. Neutron fluences ranged between 10^{11} and 10^{14} n/cm^2. GaAs detectors were exposed to exponential fluences of base ten. Ten detector designs were irradiated and studied, differentiated between p–i–n diodes and Schottky barrier diodes.

The irradiated ^{10}B-coated detectors were tested for neutron detection sensitivity in a thermalized neutron beam. Little damage was observed for detectors irradiated at neutron fluences of 10^{12} n/cm^2 and below, but signals noticeably degraded at fluences of 10^{13} n/cm^2. Catastrophic damage was apparent for neutron fluences of 10^{14} n/cm^2. Comparison studies also included semi-insulating bulk GaAs thermal neutron detectors. It was observed that the SI bulk GaAs Schottky barrier detectors sustained the highest fluences prior to device failure. The main cause of detector failure was determined to result from the ^{10}B(n,α)^{7}Li reaction product damage. © 2002 Published by Elsevier Science B.V.

Keywords: Semiconductor neutron detector; Radiation hardness

1. Introduction

Semiconductor detectors coated with thin, neutron-reactive films have been demonstrated as potentially useful devices for thermal neutron detection [1–10]. Semiconductor material candidates include bulk Si, SiC, GaAs, diamond, and amorphous Si [1–10]. The semiconductor material substrate and the neutron-reactive film should have properties that assist in discriminating between neutron interaction events and gamma-ray-induced events. Variations of Si and diamond detectors have low gamma-ray interaction

*Corresponding author. Present address: Department of Mechanical and Nuclear Engineering, Kansas State University, 318 Rathbone Hall, Manhattan, KS 66506-5205, USA. Tel.: +1-785-532-5284; fax: +1-785-532-7057.

E-mail address: mcgregor@ksu.edu (D.S. McGregor).

0168-9002/02/$ - see front matter © 2002 Published by Elsevier Science B.V.
PII: S0168-9002(02)00793-3

probabilities due to their respective low atomic numbers. The elemental constituents of GaAs have comparatively higher atomic numbers than Si and diamond, although they are still reasonably low; therefore, GaAs has been demonstrated as a viable substrate for thin-film-coated neutron detectors [5].

A low operating voltage is a desirable attribute for semiconductor devices. Both Si and GaAs can be produced with such high purity that the depletion voltage for a detector diode can be extremely low. Recently, detectors fabricated from high-purity, epitaxially grown GaAs layers demonstrated very good results under zero bias conditions [9]. The epitaxial GaAs detectors were coated with various thicknesses of pure ^{10}B films, and the ^{10}B(n,α)^{7}Li reaction was used as the basis of the neutron detection mechanism. The devices clearly exhibited thermal neutron detection with no voltage applied. Additionally, the epitaxial diode active regions ranged from only 1 to 5 μm in thickness and were so very thin that gamma-ray interactions were negligible. As a result, the detectors self-discriminated the background gamma-ray environment from thermal neutrons.

An additionally desirable attribute for a viable semiconductor neutron detector is that it will withstand the harsh radiation environment in which it will be operated. Experimental irradiations with thermal neutrons from a 2 MW materials test nuclear reactor, the Ford Nuclear Reactor (FNR), demonstrated noticeable detector performance degradation at thermal neutron fluences near 10^{13} n/cm^2 and catastrophic failure at thermal neutron fluences nearing 10^{14} n/cm^2. During the reactor irradiation, the detectors experienced damage from gamma rays, fast and thermal neutrons, and also the ^{10}B(n,α)^{7}Li reaction products from within the neutron sensitive films. It became necessary to isolate the source of the catastrophic damage, thereby allowing for improved designs. Sample sets of assorted, self-biased neutron detectors were irradiated with different fast and thermal neutron fluences from the FNR in order to determine the main cause of the catastrophic failure from the devices.

2. Theoretical considerations

2.1. ^{10}B film coatings and efficiency

The ^{10}B(n,α)^{7}Li reaction leads to the following reaction products and branching ratios [11]:

$$^{10}\mathrm{B} + n \rightarrow \begin{cases} 6\%: & ^{7}\mathrm{Li}(1.015\ \mathrm{MeV}) + \alpha(1.777\ \mathrm{MeV}) \\ & Q = 2.792\ \mathrm{MeV}\ \ (\text{to ground state}) \\ 94\%: & ^{7}\mathrm{Li}^{*}(840\ \mathrm{keV}) + \alpha(1.470\ \mathrm{MeV}) \\ & Q = 2.310\ \mathrm{MeV}\ \ (\text{1st excited state}). \end{cases}$$

The thermal neutrons (0.0259 eV) absorbed by ^{10}B produce energetic particles traveling at an 180° angle. After absorption, 94% of the reactions leave the ^{7}Li ion in its first excited state that rapidly de-excites to the ground state ($\sim 10^{-13}$ s) by releasing a 480 keV gamma ray. The remaining 6% of the reactions result in the ^{7}Li ion going directly to its ground state. The thermal neutron (0.0259 eV) microscopic absorption cross-section is 3840 b. The microscopic thermal neutron absorption cross section increases with decreasing neutron energy; thus, the cross-section dependence is proportional to the inverse of the neutron velocity ($1/v$) in much of the energy range [11,12].

Neutrons may interact anywhere within the reactive film, and the reaction products lose energy as they move through the neutron-reactive film. Reaction product self-absorption reduces the energy transferred to the semiconductor detector, and ultimately limits the maximum film thickness that can be deposited over the device's blocking contact. The measured voltage signal is directly proportional to the number of electron–hole pairs excited within the semiconductor.

The average range for a 840 keV ^{7}Li ion in boron is 1.6 μm microns, and the average range for a 1.47 MeV alpha particle is 3.6 μm. Reaction products that deposit most or all of their energy in the detector will produce much larger voltage signals than those reaction products that lose most of their energy before reaching the detector. The energy absorbed in the detector is simply the original particle energy minus the combined energy lost in the boron film and detector contact during transit [9,13].

2.2. Diode structures

From previous work [9], high-purity, undoped GaAs epitaxial layers grown onto n-type GaAs substrates were used as "self-biased" neutron detectors (Fig. 1). The self-biased concept was also demonstrated successfully with Si diodes, in conjunction with LiF converters rather than ^{10}B films [3]. The ^{10}B(n,α)^{7}Li reaction products have very short ranges in semiconductor solids, shorter than ^{6}Li(n,α)^{3}H reaction products, thereby only requiring very thin active regions for coated diode structures.

The GaAs devices [9] incorporated undoped regions grown by low-pressure metalorganic chemical vapor deposition that had background impurity concentrations of $n = 3 \times 10^{14}/\text{cm}^3$, thereby yielding unintentionally doped *v*-type GaAs material. The diodes used two blocking contact adaptations atop the high-purity *v*-type GaAs active regions: 2000 Å thick p+GaAs blocking contacts and 200 Å thick Schottky blocking contacts. The *v*-type GaAs active layers ranged between 1 and 5 μm in thickness. The devices were coated with films of 98% enriched high-purity ^{10}B. Several variations of these structures were fabricated (refer to Tables 1 and 2). For the high-purity epitaxial GaAs devices, the difference between the work functions of the blocking contacts (either p + GaAs or Schottky barrier) and the *v*-type high-purity GaAs active region produced an internal potential difference at the film interface [14]. This "built-in" potential produces an internal electric field, which thereby depletes a sufficient portion of the *v*-type GaAs region and provides sufficient charge carrier collection. Therefore, external voltage bias is not required to operate the devices. Voltage need only be applied in order to operate the supporting readout electronics.

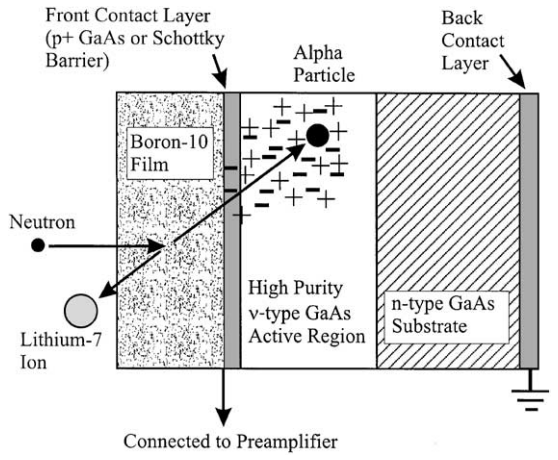

Fig. 1. The basic construction of a ^{10}B-coated self-biased high-purity epitaxial GaAs neutron detector. Neutrons interact in the ^{10}B film, thereby releasing an alpha particle and a ^{7}Li ion in opposite directions. Only one particle from the interaction can enter the detector. The built-in potential at the contact/*v*-type GaAs interface supplies enough voltage to operate the device.

Some of the Schottky-type detector diodes operated slightly better when low reverse voltages were applied, most notably type 'M' (Table 2, Spire 92). The Schottky barrier devices demonstrated expectedly higher reverse leakage currents than the p+ contact devices due to the lower barrier height generally formed by Schottky contacts in comparison to p−i−n structures. Furthermore, the previously described difference in the work functions between the p+ and the *v*-type GaAs region results in a greater built-in potential for the p−i−n structure than the Schottky barrier structure and an accordingly greater internal electric field.

The assorted detector diodes are being studied for the potential application to the fields of remote neutron sensing and thermal neutron imaging. In both cases, it is beneficial to eliminate the operating bias requirement. Mainly, remote sensing requires low power consumption as is accomplished with the self-biased configuration. Remote neutron detection, if the devices are to be used in hostile environments, may require that the devices withstand extreme radiation environments. Also, for the devices to become viable thermal neutron beam monitors they must be able to withstand the harsh environment produced from a variety of neutron sources, such as a nuclear reactor, a solid source, or a generator. In order to ascertain their radiation hardness, the devices of this study have been exposed to a variety of radiations, consisting of systematic and incremental doses of gamma rays, fast and thermal

Table 1
Collection One of high-purity GaAs diodes investigated as neutron detectors

Sample number	Diode type	^{10}B film thickness (Å)	Blocking contact (Å)	ν-type GaAs ($n = 3 \times 10^{14}/cm^3$)	Intermediate layer	Substrate
3241	p–i–n	5000	p+GaAs ($2 \times 10^{19}/cm^3$) 2000	5 μm thick	None	n-type GaAs
3243	p–i–n	7200	p + GaAs ($2 \times 10^{19}/cm^3$) 2000	5 μm thick	None	n-type GaAs
3246	p–i–n	5000	p + GaAs ($2 \times 10^{19}/cm^3$) 2000	1 μm thick	None	n-type GaAs
3247	p–i–n	5000	p + GaAs ($2 \times 10^{19}/cm^3$) 2000	2 μm thick	n-type $Al_xGa_{1-x}As$ ($5 \times 10^{15}/cm^3$) 2500 Å	n-type GaAs
3278	Schottky diode	6500	Au Schottky barrier 200	5 μm thick	None	n-type GaAs

Table 2
Collection Two of various detector diodes investigated as neutron detectors

Sample letter (number)	Diode type	^{10}B film thickness (Å)	Blocking contact (Å)	ν-type GaAs ($n = 3 \times 10^{14}/cm^3$)	Intermediate layer	Substrate
A	Schottky diode	5000	Ti/Au Schottky 550	None	None	SI Bulk GaAs
E (Spire 76)	GaAs p–i–n diode	5000	p + GaAs ($2 \times 10^{19}/cm^3$) 1000	5 μm thick	None	n-type GaAs
I (Spire 88)	GaAs Schottky diode	5000	Au Schottky contact 200	5 μm thick	None	n-type GaAs
K (Spire 89)	GaAs Schottky diode	5000	Au Schottky contact 200	5 μm thick	None	n-type GaAs
M (Spire 92)	GaAs Schottky diode	5000	Au Schottky contact 200	5 μm thick	n-type $Al_xGa_{1-x}As$ ($5 \times 10^{15}\,cm^3$)2500 Å	n-type GaAs

neutrons, and reaction product charged particles from $^{10}B(n,\alpha)^7Li$ reactions.

For comparison purposes, bulk SI GaAs devices were fabricated as well. The GaAs devices were lapped and etched to thicknesses between 200 and 250 μm and were fabricated as Schottky barrier diodes [15]. As with the epitaxial devices, the bulk GaAs detectors were also coated with films of 98% enriched high-purity ^{10}B. The SI Bulk GaAs detectors have much lower built-in potentials than the epitaxial devices and therefore required 100 V reverse bias for operation. The operating reverse bias appears higher than quoted in literature elsewhere [15], yet the high reverse voltage was required because of the resistance divider circuit within the preamplifier (Ortec 142A) used for the measurements. The actual voltage applied across the SI bulk GaAs diodes ranged only from 10 to 15 V.

3. Experimental arrangement

A variety of detectors were exposed in the moderator pool near the FNR to accelerate radiation damage and determine the radiation hardness of each detector configuration. The assorted sample detector configurations are

delineated in Tables 1 and 2. As seen in both tables, two detector *collections* were studied. A set of control sample detectors from each collection was *non*-irradiated so as to serve as a reference.

The first collection of detectors was irradiated in the moderator pool of the 2 MW FNR. The ^{10}B-coated devices were exposed to gamma rays, thermal and fast neutrons, and to the charged particles produced from the $^{10}B(n,\alpha)^{7}Li$ reaction, and no attempt was made with the first collection to separate the damage effects from the different radiation types. The irradiated detectors of Collection One consisted of five sample detectors fabricated on n-type GaAs substrates and divided into two diode types (each with its associated blocking contact). Four of the sample detectors were p−i−n diodes and one was a Schottky diode. Specific characteristics that distinguish the sample detectors include variable thickness of the applied 98% ^{10}B film layer and of the *v*-type epitaxial GaAs region (Table 1). The five sample detectors were further divided into four sets, defined by the four total neutron fluences to which the epitaxial detectors were exposed. Sample detector sets were irradiated at fixed grid locations near the core of the aforementioned 2 MW research reactor so as to ensure conditions of identical reactor fuel configuration. Additionally, the fast-to-thermal neutron flux was kept as similar as possible for each increment in neutron fluence. The sample sets were placed in moisture-proof aluminum irradiation cartridges and were fastened to an internal aluminum fixture so that irradiation would be spatially consistent in reference to the reactor flux. Gold foils and iron wires were located within each cartridge to monitor the total neutron exposure and later measured to confirm the total slow and fast neutron fluences received. Total neutron fluences ranged between 7.0×10^{11} and 7.63×10^{13} n/cm^2 with incremental factors of approximately ten (Table 3). In addition to thermal and fast neutrons, the detectors experienced radiation damage from gamma rays and charged-particle reaction products from $^{10}B(n,\alpha)^{7}Li$ reactions. It was observed from Collection One that catastrophic damage occurred to all sample detectors for neutron fluences exceeding 10^{13} n/cm^2. Of the configurations, device samples from 3278 (Schottky barrier devices) demonstrated failure at the lowest neutron fluences. Unfortunately, since the detectors were simultaneously exposed to gamma rays, slow and fast neutrons, and resultant $^{10}B(n,\alpha)^{7}Li$ charged particles in the reactor pool, determining the type of radiation that contributed most to device failure was not possible.

Table 3
Measured neutron fluences to which the first collection of detectors was subjected

Sample set	Thermal neutron fluence (n/cm^2)	Fast neutron fluence (n/cm^2)	Total neutron fluence (n/cm^2)
1	None	None	None
2	4.58×10^{11}	2.43×10^{11}	7.01×10^{11}
3	4.98×10^{12}	2.65×10^{12}	7.63×10^{12}
4	4.98×10^{13}	2.65×10^{13}	7.63×10^{13}

An experiment was then designed to determine which form of radiation caused the catastrophic damage. The second collection of detectors in Table 2 was irradiated under altered experimental parameters in order to isolate the type of radiation predominantly responsible for detector damage and failure. The irradiated detectors of Collection Two consisted of five sample detectors divided into four diode types (each with its associated blocking contact). The specific characteristics that primarily distinguish the sample detectors include dissimilar substrates and either the presence or the absence of the *v*-type epitaxial GaAs active region. All sample detectors were further classified into three sets, defined by the ^{10}B layer. Sample detectors in Sets One and Three were coated with 5000 Å of ^{10}B, while sample detectors in Set Two were uncoated. Numerous representative detectors of each sample detector cited in Table 2 were present in all three sets. Additionally, each set was subdivided into five subsets. The subsets were defined by the five total neutron fluences to which all sets of the sample detectors were exposed (Table 4).

Numerous representative detectors from each sample detector cited in Table 2 and from each of the three sets were present in all five subsets. Irradiation procedures were performed as those

Table 4
Measured gamma-ray doses and neutron fluences to which the second collection of detectors was subjected

Subset	Thermal neutron fluence (n/cm^2)	Fast neutron fluence (n/cm^2)	Total neutron fluence (n/cm^2)	γ-ray exposure (rad)
Set 1 (^{10}B-coated) and Set 2 (uncoated)				
1	None	None	None	None
2	1.0×10^{11}	5.1×10^{10}	1.51×10^{11}	2.99×10^{4}
3	1.1×10^{12}	5.4×10^{11}	1.6×10^{12}	2.39×10^{5}
4	9.3×10^{12}	4.6×10^{12}	1.4×10^{13} [a]	2.24×10^{6}
5	8.9×10^{13}	4.4×10^{13}	1.3×10^{14}	1.89×10^{7}
Set 3 (^{10}B-coated)				
1	None	None	None	None
2	None	None	None	2.41×10^{4}
3	None	None	None	2.44×10^{5}
4	None	None	None	2.27×10^{6}
5	None	None	None	1.85×10^{7}

[a] Sample detectors M received a measured neutron fluence of 1.6×10^{13} n/cm^2.

previously described for all the detectors in Collection One, and gold foils were placed with each sample subset to monitor the total neutron fluence. Sets One and Two were irradiated *together* in the reactor moderator pool so that each subset experienced a tenfold increase in neutron fluence over the previous subset. Since Sets One and Two were irradiated in the same reactor pool locations at the same time, the neutron fluences experienced by each are identical. The third detector set was irradiated in the Phoenix Memorial Laboratory ^{60}Co Irradiator Facility so that the calculated gamma-ray doses correspond with the doses received by detector Sets One and Two whilst in the reactor pool. The uncoated samples of Set Two were later coated with 5000 Å of 98% ^{10}B after the reactor pool irradiations were complete, thereby allowing for a direct comparison in device performance to the other two sets. As a consequence of manipulating research parameters, Set One was subjected to gamma-ray, neutron, and charged-particle damage, Set Two only to gamma-ray and neutron damage, and Set Three only to gamma-ray damage. In summary, the ^{10}B-coated devices underwent damage from gamma rays, thermal and fast neutrons, and charged particles resulting from ^{10}B(n,α)^{7}Li reactions. The uncoated devices, however, experienced damage only from gamma rays and neutrons; the uncoated devices did not undergo damage from ^{10}B(n,α)^{7}Li reaction charged particles since they did not have ^{10}B coatings.

The neutron-produced, radioactive reaction products (mainly activated Au from the contacts) were allowed to decay to minimal levels before the detectors were tested. Afterward, the detectors were sealed in light impenetrable, self-aligning aluminum boxes [9] for testing that shielded them from radiofrequency and photoelectric noise. The boxes were also designed to incorporate cylindrical, close-ended, hollow chimneys on the obverse and reverse, enabling repeatable indexing of the detector's location in the thermal neutron beam. The devices were tested by placing them in a diffracted thermalized neutron beam in a port at the 2 MW Ford Nuclear Reactor (Fig. 2) [9]. The diffracted beam substantially reduced the gamma-ray background during the measurements, hence the pulses observed were primarily from ^{10}B(n,α)^{7}Li reactions in the detector films.

Sample detectors from Collection One were placed in a doubly diffracted thermal neutron beam (Position 2 in Fig. 2) and all detectors were operated under zero bias conditions. Thermal neutron measurements employing a fission chamber yielded an estimated flux of 2×10^4 n/cm^2 s. One-hour measurements were conducted, and the ^{10}B(n,α)^{7}Li reaction product spectrum was recorded for each sample detector irradiated with the specified fluences.

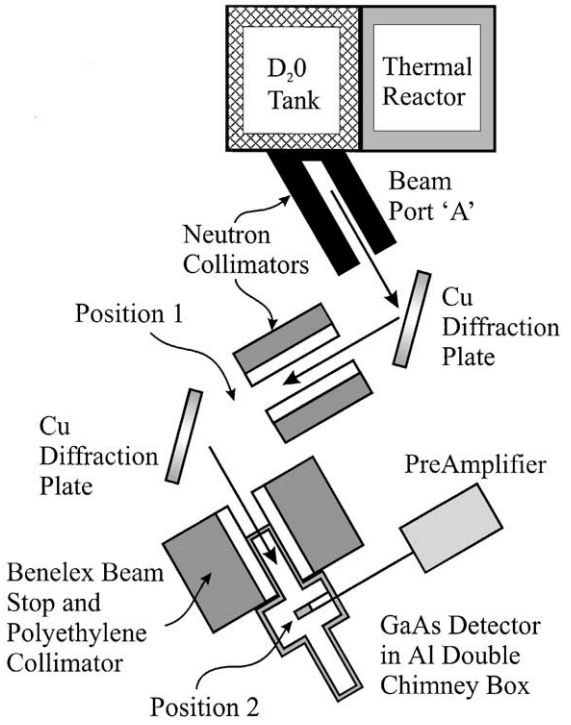

Fig. 2. Experimental configuration for thermal neutron detection with the various detector diode devices. The aluminum chimney box ensured consistent alignment within the neutron beam.

Sample detectors from Collection Two were placed in a singly diffracted thermal neutron beam (Position 1 in Fig. 2) for 15 min measurements. A non-irradiated control detector from each of the sample detector sets and subsets was first tested. For all control detectors, the operating voltage and gain were adjusted and documented such that the 1.47 MeV alpha particle peak centroids lie at channel number 1000. For all subsequent sample detectors, the voltage and gain were re-adjusted to the values documented from the control sample detectors corresponding to the same type and set. Allowing for some hysteresis, the procedure permitted a direct comparison of device degradation between the detector diode types. The spectra from each sample detector diode type and collection were recorded and the changes notated. The peak shift and the total number of counts in the peaks (both 840 keV ^{7}Li ion and 1.47 MeV alpha particle) were documented and compared, giving a standard of measure for detector degradation.

4. Results

4.1. Collection One

The damage is distinctively noticeable for the Schottky barrier diodes at neutron fluences of 7×10^{11} n/cm^2. However the p−i−n diode shows little change for the same neutron fluence. Fig. 3 shows the pulse height spectra for p−i−n diode detectors of sample 3246, and Fig. 4 shows pulse height spectra for Schottky diodes of sample 3278.

The neutron-induced count rate provides another comparative gauge for results. The normalized neutron-induced counts for all the sample detectors as a function of neutron fluence appear in Fig. 5. Sample detector diodes 3246 and 3247 show the least operational degradation, while the other devices show total catastrophic failure (no pulses) above a neutron fluence of 7.6×10^{13} n/cm^2. These data are based on measured and tabulated fast and thermal neutron fluences in Table 3. The distinctive difference between diode styles 3246, 3247, and the remainder diodes is the *v*-type high-purity GaAs region thickness. Diode style 3246

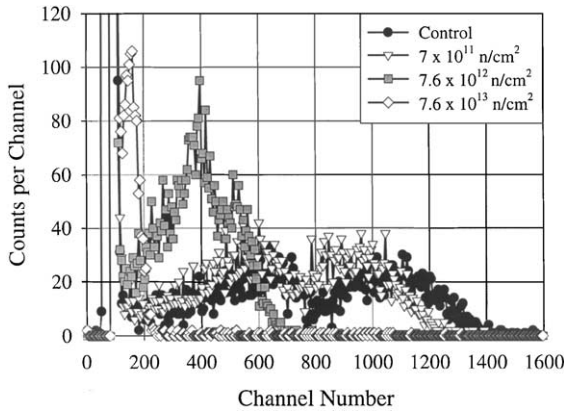

Fig. 3. Pulse height spectra as a function of neutron fluence from sample detector diode configuration 3246 of thermal neutron reactions in ^{10}B. The diodes were operated under zero bias conditions.

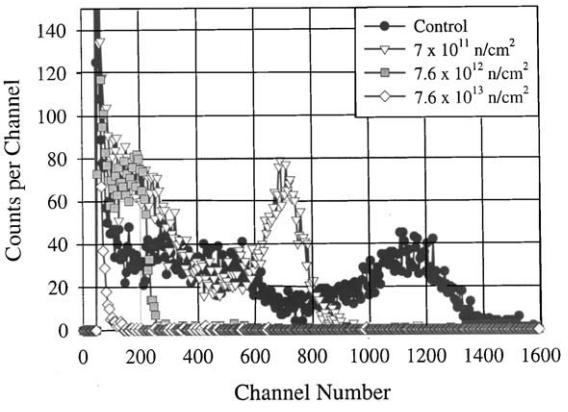

Fig. 4. Pulse height spectra as a function of neutron fluence from sample detector diode configuration 3278 of thermal neutron reactions in ^{10}B. The diodes were operated under zero bias conditions.

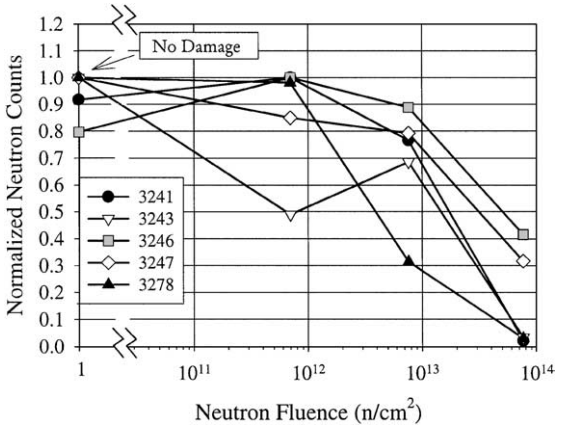

Fig. 5. Normalized neutron-induced counts for various detector types as a function of neutron fluence. Degradation is less prominent for detector configurations 3246 and 3247, which consist of the thinnest epitaxial GaAs layers of the p–i–n diodes.

has a 1 μm thick *v*-type high-purity region, diode style 3247 has a 2 μm thick *v*-type high-purity region, and the remainder (3241, 3243 and 3278) all have 5 μm thick *v*-type high-purity regions. Overall, the p–i–n diodes performed similarly. Diode type 3278 was the only Schottky contact device type, which has a lower blocking barrier height and resultant built-in potential than the p–i–n diode structures. It is very possible, due to the lower internal voltage, that displacement damage sites caused charge carrier trapping more effectively in the Schottky barrier devices than the p–i–n devices, which may explain their observed failure at lower neutron fluences than observed for the p–i–n devices.

The information acquired from Collection One identified the irradiation region of interest, in which damage was observed to occur between thermal neutron fluences of 10^{12} and 10^{14} n/cm^2. Since the devices experienced radiation damage from gamma rays, neutrons, and charged-particle reaction products at the same time, it became important to identify the form of radiation most responsible for the observed device failure. The irradiation procedure for samples from Collection Two was designed to separate the damage effects of the different forms of radiation.

4.2. Collection Two

4.2.1. Gamma-ray irradiation

Set Three consisted of five distinct sample detectors of one detector diode type each (Table 2). Each detector had 5000 Å of ^{10}B film on the blocking contact, and each detector was mounted with silver epoxy on alumina (Al_2O_3) substrate plates, the latter employed as a mount for the detectors in the aluminum chimney test boxes. All five of the sample detectors were placed into basic, laboratory-grade plastic wafer holders and inserted into the central region of a 20 kCi ^{60}Co gamma-ray chamber. The devices were completely surrounded by the ^{60}Co source. Irradiations ranged from 2.4×10^4 to 1.8×10^7 rad (calibrated with a Reuter–Stokes model RS-C4-1606-207 ionization chamber), and the dose increments were intentionally matched to the gamma-ray doses experienced by the detectors irradiated in the reactor pool. Following each gamma-ray dose, the devices were tested in the diffracted neutron beam, after which they were reinserted into the ^{60}Co chamber to receive a tenfold increase in gamma-ray exposure before the next incremented test measurement.

Fig. 6a shows the results for sample detectors 'E' (Spire 76), in which the neutron reaction product spectra are plotted according to total gamma-ray

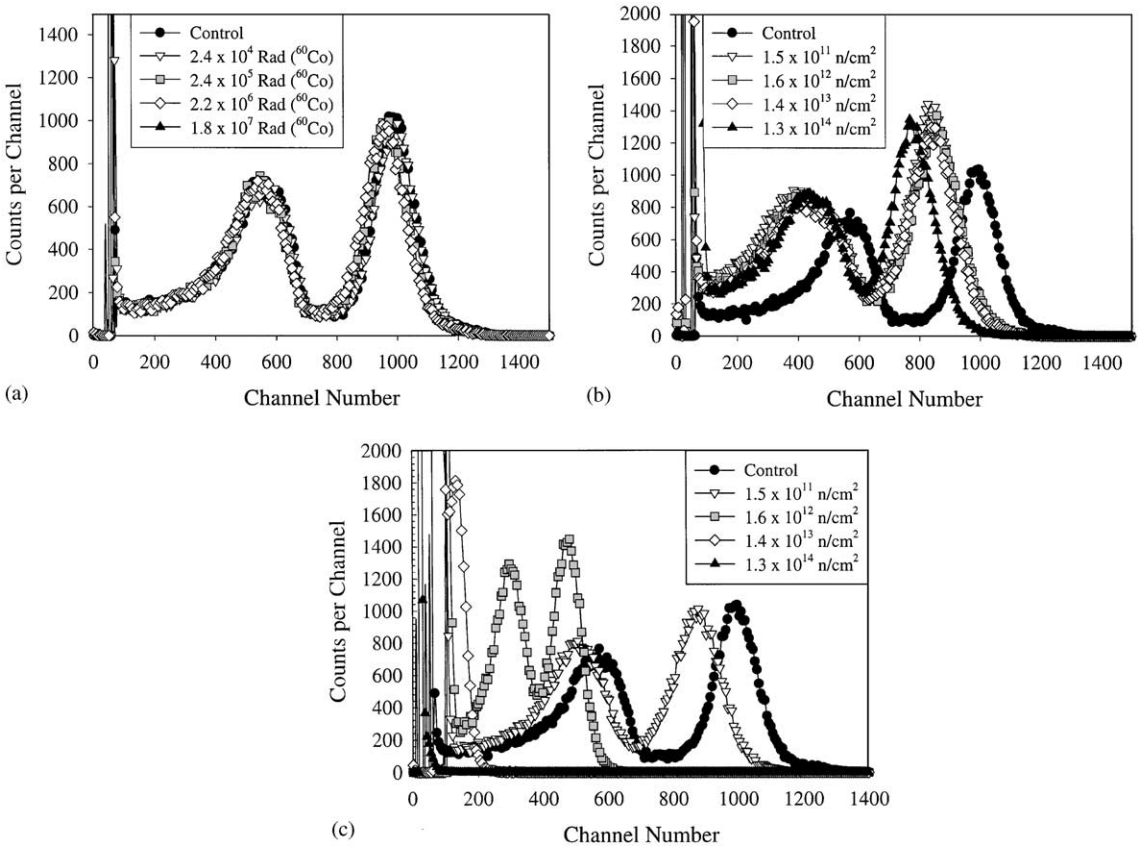

Fig. 6. Pulse height spectra for detector diodes of type E as a function of (a) gamma-ray dose, (b) thermal and fast neutron fluence on bare detectors, and (c) thermal and fast neutron fluence on ^{10}B-coated detectors. The diodes were operated under zero bias conditions. Devices with ^{10}B-coating before neutron irradiation suffered damage from charged-particle reaction products.

dosage. Shown are the changes in spectra as a function of gamma-ray doses received in a ^{60}Co irradiator chamber. It is important to note that there is very little change in the spectra for the detectors, which indicates that the gamma-ray irradiations had minimal effect on performance. Fig. 7a shows the results for sample detectors 'M' as biased at -40 V and Fig. 8a shows the results for sample detectors 'A' as biased at -100 V. Both sample types 'M' and 'A' seem unaffected by the gamma radiation. All other detectors represented in Table 2 experienced similar results, in which the pulse height spectrum showed very little change for the different doses of gamma rays. The detectors operate as counters, therefore stability in the total spectral neutron count rate is most important. Fig. 9 shows the total neutron spectral counts as normalized to the control detector of the same diode type. Very little deviation in the count rate may be distinguished. Some slight manual errors in bias and gain settings may have contributed to the differences noted. Regardless, the spectral deviations and count rate differences are minimal. For this reason it is unlikely that gamma rays are responsible for the catastrophic failure of the devices.

4.2.2. *Slow and fast neutron irradiation*

Sample detector Set Two consisted of five subsets in which samples of each diode type (Table 2) were within the subsets. Hence, unlike sample Set Three where the same detectors were repeatedly irradiated, *different* detectors from the same fabrication batch were irradiated for each

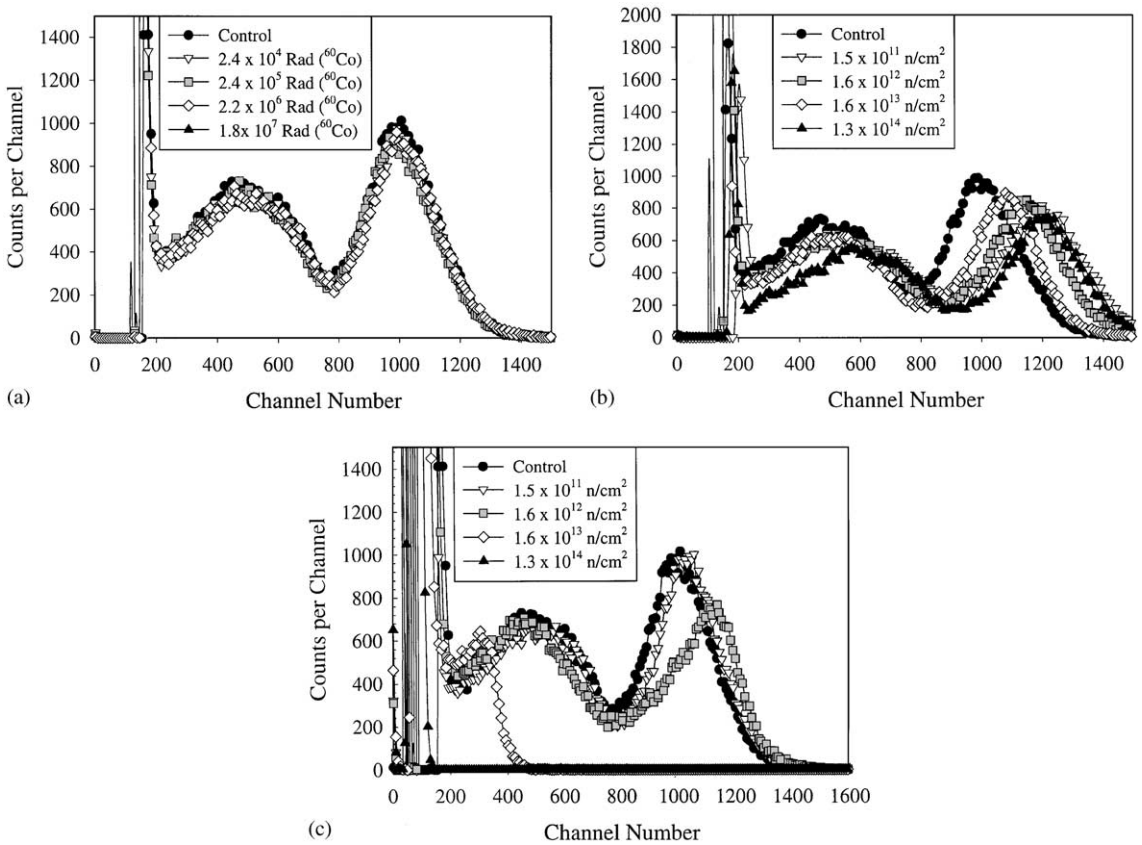

Fig. 7. Pulse height spectra for detector diodes of type M as a function of (a) gamma-ray dose, (b) thermal and fast neutron fluence on bare detectors, and (c) thermal and fast neutron fluence on ^{10}B-coated detectors. The diodes were operated at -40 V reverse bias. Devices with ^{10}B-coating before neutron irradiation suffered damage from charged-particle reaction products.

radiation increment. The procedure was found necessary to eliminate neutron activation of the sample mounts. Each subset received a different neutron fluence that was monitored and recorded by the Au foils included with the detectors in the irradiation cartridges. For high neutron fluences, Fe wires were included with the Au foils as well. The total slow and fast neutron fluences ranged from 1.5×10^{11} to 1.3×10^{14} n/cm^2 (Table 4). Hence, the devices were exposed to both gamma ray and neutron damage but not to ^{10}B(n,α)^{7}Li reaction product damage. Following irradiation, a 5000 Å film of ^{10}B was deposited on the detector blocking contacts to observe the neutron detection performance.

The gamma-ray doses for Set Two were similar to those doses experienced by sample Set Three in the ^{60}Co gamma-ray chamber (refer Table 4). Consequently, the detectors of sample Set Two were exposed to the same gamma-ray increments as sample Set Three and were also exposed to the neutron fluences described in the preceding paragraph and are shown in Table 4. As discussed earlier, they were coated with ^{10}B *after* irradiation, thereby eliminating the damage contribution from the ^{10}B(n,α)^{7}Li reaction products. Fig. 6b shows spectra for detector diodes 'E' from Set Two plotted according to the total neutron fluence received. Similar to sample Set Three, the spectra do not reflect appreciable spectral changes with increasing neutron fluence. All other detectors from Set Two demonstrated similar results in which very little difference was noted in the reaction product spectra for the various radiation

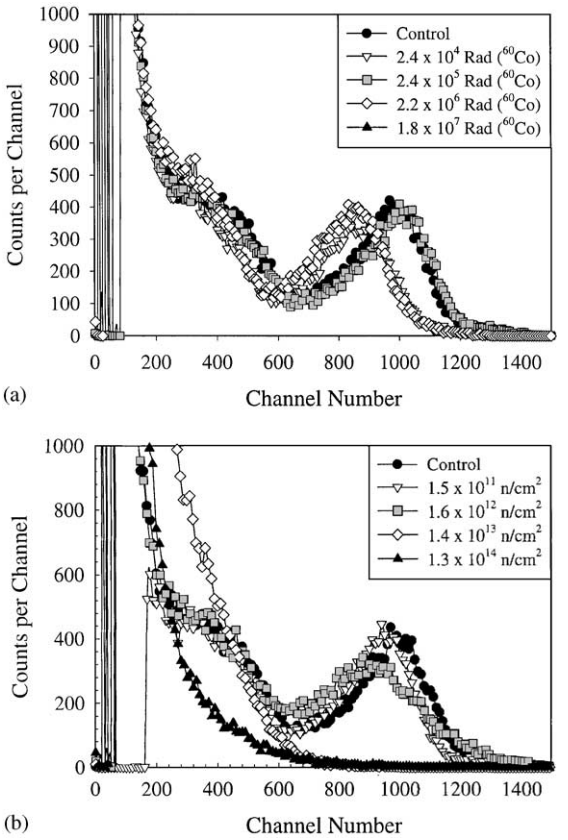

Fig. 8. Pulse height spectra for detector diodes of type A as a function of (a) gamma-ray dose and (b) thermal and fast neutron fluence on ^{10}B-coated detectors. The diodes were operated at -100 V reverse bias. Devices with ^{10}B-coating before neutron irradiation suffered damage from charged-particle reaction products.

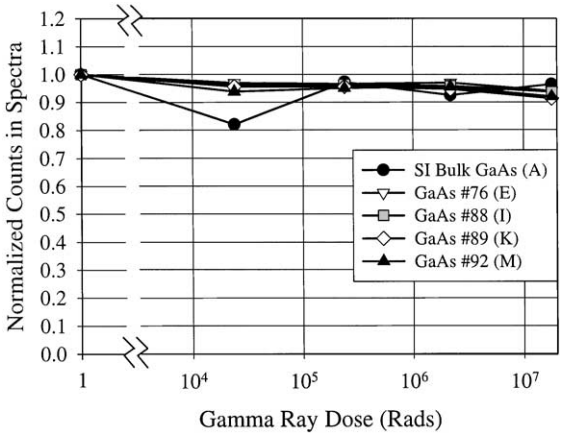

Fig. 9. Changes in the normalized total neutron-induced counts for various detector types as a function of gamma-ray dose.

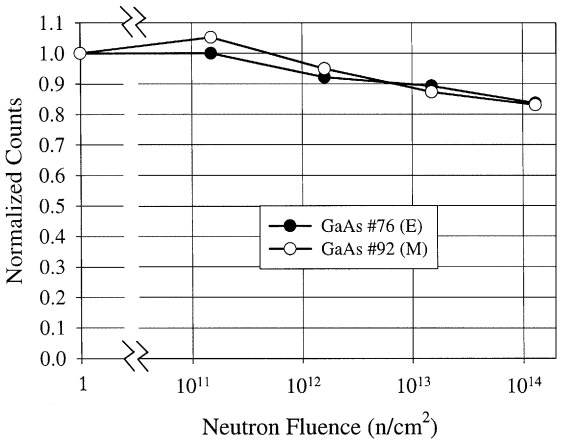

Fig. 10. Changes in the normalized total neutron-induced counts for detector types E and M as a function of neutron fluence. The devices were bare (uncoated) during the irradiation procedure.

exposures. For instance, Fig. 7b shows the results from detector diodes of type 'M' (at a bias of -40 V), showing little difference for the various spectra.

The slight spectral changes observed in Figs. 6b and 7b are most likely due to characteristic differences between the separate diodes and trivial manual error in the bias and gain settings. Some small degree of change perhaps may be due to neutron damage, and Fig. 10 indicates that there is a decreasing trend in the neutron count rate with increasing neutron fluence. However, the devices continue to work well even at fluences in the 10^{14} n/cm^2 range. Regardless, the spectral deviations and count rate differences are minimal and are clearly unlike the changes observed in Figs. 3–5 for Collection One. It is therefore unlikely that neutron exposure, for both fast and thermal neutrons, is responsible for the observed catastrophic failure of the devices in Collection One at neutron fluences near 10^{13} n/cm^2.

4.2.3. $^{10}B(n,\alpha)^7Li$ reaction product irradiation

Sample detector Set One was similar to sample Set Two, in that both sets were irradiated together in the reactor moderator pool and therefore

received identical neutron fluences. The main difference between sample Set One and Set Two was that the detector diodes in sample Set One were coated with a 5000 Å film of ^{10}B *before* neutron irradiation. As a result, detectors from sample Set One received damage from gamma rays, fast and thermal neutrons, and the $^{10}B(n,\alpha)^{7}Li$ reaction products.

Figs. 6c, 7c and 8b show the thermal neutron reaction product spectra for sample detector diode types 'E', 'M', and 'A' as plotted according to total neutron fluence. The effect of damage at fluences of 1.4×10^{13} n/cm^2 and greater is unmistakable. Since the uncoated devices did not manifest such damage, it becomes evident that the ^{10}B film is responsible for the change. It is deduced that the charged-particle emissions from the $^{10}B(n,\alpha)^{7}Li$ reactions are causing the observed damage effects. From previous work, a 5000 Å thick ^{10}B film yields a detection efficiency of about 2%, mainly because only 2% of the intersecting neutrons cause charged-particle reaction products to enter the detector [9,13]. Since the onset of catastrophic failure is observed at neutron fluences near 1.4×10^{13} n/cm^2, one can deduce that it is actually the exposure to approximately 2×10^{11} charged-particle reaction products (alpha particles and ^{7}Li ions) per square centimeter that causes the catastrophic damage to the devices. Also, since neutron detection efficiency increases with ^{10}B film thickness, which results in more charge particles entering the device, the neutron fluence catastrophic failure limit will *increase* for thinner ^{10}B films and it will *decrease* with for thicker ^{10}B films, an important fact to consider.

Fig. 11 shows a count rate comparison of all diode types from Table 2. Bulk SI GaAs Schottky barrier devices (type 'A') appear to withstand the highest fluences. Although the added radiation hardness of bulk SI GaAs may be due to the high density of surface states and deep level defects generally found with the material, the extended performance is most likely due to the external bias applied to the devices (−100 V). Nevertheless, they too underwent catastrophic damage at neutron fluences above 1.4×10^{13} n/cm^2. High-purity epitaxial GaAs p−i−n diode devices and high-purity epitaxial GaAs Schottky barrier devices performed

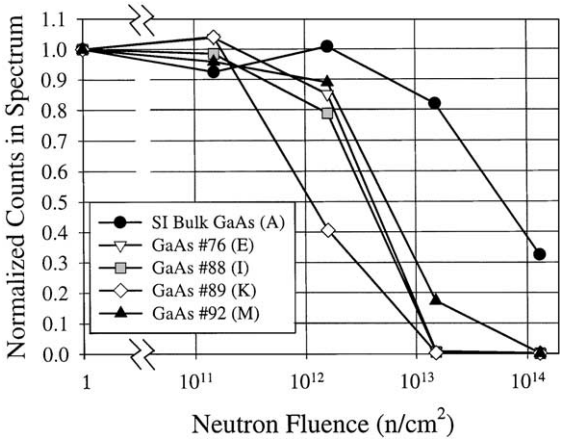

Fig. 11. Normalized total neutron-induced counts for all detector diode types in Collection Two as a function of neutron fluence. Type A detectors (SI bulk GaAs) show the greatest radiation hardness, most likely a result of the higher operating voltage. It is deduced that the $^{10}B(n,\alpha)^{7}Li$ reaction products caused the degradation shown.

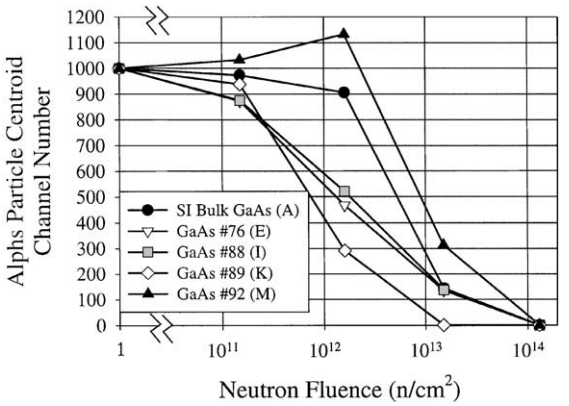

Fig. 12. Spectral centroid location for alpha-particle reaction products (from $^{10}B(n,\alpha)^{7}Li$ reactions) as a function of neutron fluence. It is deduced that the $^{10}B(n,\alpha)^{7}Li$ reaction products caused the degradation shown.

similarly, and they failed at the lowest neutron fluences.

Fig. 12 shows the 1.47 MeV peak centroid position as a function of neutron fluence. All devices showed considerable changes at 1.4×10^{13} n/cm^2, however detector diode 'M' (an epitaxial Schottky diode) unexpectedly demonstrated the least amount of change. It should be noted that diode type 'M' devices required −40 V

reverse bias to operate, which (as with the bulk GaAs devices) most likely helped to increase their tolerance level. Type 'M' devices also demonstrated the highest leakage currents of all tested devices.

5. Conclusions

The self-biased design offers a straightforward method to produce low-cost, lightweight, compact, and low-power thermal neutron detectors for remote deployment. The design also can be pixelated for neutron imaging devices. Nonetheless, the environment near a thermal or fast neutron source is generally very hostile for semiconductor detectors. The irradiation results clearly indicate that the detectors are substantially radiation resistant to gamma rays, thermal neutrons, and fast neutrons. However, the devices undergo catastrophic failure when exposed to charged-particle reaction products from $^{10}B(n,\alpha)^{7}Li$ reactions. With 2% detection efficiency for 5000 Å ^{10}B films [9,13], it presently appears that it is the exposure to approximately 10^{13} n/cm^2, which correlates to 2×10^{11} charged-particle reaction products (alpha particles and ^{7}Li ions) per square centimeter, that causes failure to the devices. These findings are consistent with previous work with both low-energy charged-particle irradiation and gamma-ray irradiation (^{60}Co) of GaAs substrates [16–19].

The damage produced by the charged-particle reaction products most likely introduces electron and hole traps into the active region, thereby reducing charge carrier mean free drift times [20–22] and compromising the built-in potential for self-biasing. Reduction in charge carrier mean free drift times and internal bias voltage both contribute to reduced charge collection efficiency, which would manifest itself as a steady reduction in observed pulse height [20–22], as observed. Such a hypothesis is supported by the fact that the devices that were operated with external bias withstood the highest neutron fluences before catastrophic failure. Since the detectors operate by sensing the 1.47 MeV alpha particles and the 840 keV ^{7}Li ions, it is mandatory that they withstand damage inflicted by these reaction products. At present the cause of damage has not been investigated, although it suspected that the semiconductor contact and surface region is becoming highly non-crystalline due to atom displacement and void formation. Such a conclusion seems logical since the $^{10}B(n,\alpha)^{7}Li$ reaction products have very short ranges in GaAs, those being 2.1 μm for 840 keV ^{7}Li ions and 4.2 μm for 1.47 MeV alpha particles [5]. However, the precise nature of the charged-particle damage from the irradiated, self-biased ^{10}B-coated high-purity epitaxial GaAs neutron detectors has, as yet, not been thoroughly investigated. Future studies will be directed toward understanding the exact mechanism of detector diode device failure and toward advanced designs that will supercede the present limitations.

Acknowledgements

This research was performed under appointment to the US Department of Energy Nuclear Engineering and Health Physics Fellowship Program sponsored by DOE's Office of Nuclear Energy, Science, and Technology. The presented work was partially funded by the following grants: Argonne National Laboratory Subcontract (DOE) 991262402 and DOE Nuclear Engineering Education and Research Grant DE-FG07-98ID13633.

The neutron detectors were fabricated at the Spire Corporation as well as at the University of Michigan in the Solid State Electronics Laboratory (SSEL) and the Semiconductor Materials And Radiological Technologies (SMART) Laboratory. Testing of the devices was performed at the Ford Nuclear Reactor at the University of Michigan.

We thank Mr. Andrew Cook at the Phoenix Memorial Laboratory and Ford Nuclear Reactor for his invaluable assistance with the detector irradiation procedures.

References

[1] A. Rose, Nucl. Instr. and Meth. 52 (1967) 166.
[2] B. Feigl, H. Rauch, Nucl. Instr. and Meth. 61 (1968) 349.

[3] S. Pospisil, B. Sopko, E. Harrankova, Z. Janout, J. Konicek, I. Macha, J. Pavlu, Radiat. Prot. Dosim. 46 (1993) 115.
[4] A. Mireshghi, G. Cho, J.S. Drewery, W.S. Hong, T. Jing, H. Lee, S.N. Kaplan, V. Perez-Mendez, IEEE Trans. Nucl. Sci. NS-41 (1994) 915.
[5] D.S. McGregor, J.T. Lindsay, C.C. Brannon, R.W. Olsen, IEEE Trans. Nucl. Sci. NS-43 (1996) 1357.
[6] C. Petrillo, F. Sacchetti, O. Toket, N.J. Rhodes, Nucl. Instr. and Meth. A 378 (1996) 541.
[7] A.R. Dulloo, F.H. Ruddy, J.G. Seidel, Radiation response testing of silicon carbide semiconductor neutron detectors for monitoring thermal neutron flux, Report No. 97-9TK1-NUSIC-R1, Westinghouse STC, 1997.
[8] F. Foulon, P. Bergonzo, A. Brambilla, C. Jany, B. Guizard, R.D. Marshall, Proc. MRS 487 (1998) 591.
[9] D.S. McGregor, S.M. Vernon, H.K. Gersch, S.M. Markham, S.J. Wojtczuk, D.K. Wehe, IEEE Trans. Nucl. Sci. NS-47 (2000) 1364.
[10] A.J. Peurrung, Nucl. Instr. and Meth. A 443 (2000) 400.
[11] G.F. Knoll, Radiation Detection and Measurement, 3rd Edition, Wiley, New York, 2000.
[12] D.I. Garber, R.R. Kinsey, BNL 325: Neutron Cross Sections, Curves, Vol. 2, 3rd Edition, Brookhaven National Laboratory, Upton, 1976.
[13] D.S. McGregor, R.T. Klann, H.K. Gersch, Y-H. Yang, Nucl. Instr. and Meth. A 466 (2001) 126.
[14] S.M. Sze, Physics of Semiconductor Devices, 2nd Edition, Wiley, New York, 1981.
[15] D.S. McGregor, J.E. Kammeraad, Semiconductors for room temperature nuclear detector applications, in: T.E. Schlesinger, R.B. James (Eds.), Semiconductors and Semimetals, Vol. 43, Academic Press, San Diego, 1995 Chapter 10)..
[16] J.M. Borrego, R.J. Gutmann, S. Ashok, IEEE Trans. Nucl. Sci. NS-23 (1976) 1671.
[17] D.M. Newell, P.T. Ho, R.L. Menick, J.R. Pelose, IEEE Trans. Nucl. Sci. NS-28 (1981) 4403.
[18] S.P. Beaumont, et al., Nucl. Instr. and Meth. A 322 (1992) 472.
[19] W. Karpinski, T. Kubicki, K. Lubelsmeyer, M. Toporowsky, W. Wallraff, K. Heime, R. Wuller, Nucl. Instr. and Meth. A 323 (1992) 635.
[20] R.B. Day, G. Dearnaley, J.M. Palms, IEEE Trans. Nucl. Sci. NS-14 (1967) 487.
[21] W. Akutagawa, K. Zanio, J. Appl. Phys. 40 (1969) 3838.
[22] G.F. Knoll, D.S. McGregor, Proc. MRS 301 (1993) 3.